



# Numerical Homogenization of the Absolute Permeability Using the Conformal-Nodal and Mixed-Hybrid Finite Element Method

WOUTER ZIJL<sup>1</sup> and ANNA TRYKOZKO<sup>2</sup>

<sup>1</sup>*Netherlands Institute of Applied Geoscience TNO, P.O. Box 80015, NL-3508 TA Utrecht, The Netherlands, e-mail: w.zijl@nitg.tno.nl*

<sup>2</sup>*Warsaw University of Technology, ul. Nowowiejska 20, PL-00-653 Warsaw, Poland, e-mail: anna.trykozko@is.pw.edu.pl*

(Received: 6 July 1999; in final form: 6 July 1999)

**Abstract.** The modeling of hydrocarbon reservoirs and of aquifer-aquitard systems can be separated into two activities: geological modeling and fluid flow modeling. The geological model focuses on the geometry and the dimensions of the subsurface layers and faults, and on its rock types. The fluid flow model focuses on quantities like pressure, flux and dissipation, which are related to each other by rock parameters like permeability, storage coefficient, porosity and capillary pressure. The absolute permeability, which is the relevant parameter for steady single-phase flow of a fluid with constant viscosity and density, is studied here. When trying to match the geological model with the fluid flow model, it generally turns out that the spatial scale of the fluid flow model is built from units that are at least a hundred times larger in volume than the units of the geological model. To counter this mismatch in scales, the fine-scale permeabilities of the geological data model have to be ‘upscaled’ to coarse-scale permeabilities that relate the spatially averaged pressure, flux and dissipation to each other. The upscaled permeabilities may be considered as ‘complicated averages,’ which are derived from the spatially averaged flow quantities in such a way that the continuity equation, Darcy’s law and the dissipation equation remain valid on the coarse scale. In this paper the theory of upscaling will be presented from a physical point of view aiming at understanding, rather than mathematical rigorousness. Under the simplifying assumption of spatial periodicity of the fine-scale permeability distributions, homogenization theory can be applied. However, even then the spatial distribution of the permeability is generally so intricate that exact solutions of the homogenized permeability cannot be found. Therefore, numerical approximation methods have to be applied. To be able to estimate the approximation error, two numerical methods have been developed: one based on the conventional nodal finite element method (CN-FEM) and the other based on the mixed-hybrid finite element method (MH-FEM). CN-FEM gives an upper bound for the sum of the diagonal components of the homogenized mobility matrix, while MH-FEM gives a lower bound. Three numerical examples are presented.

**Key words:** absolute permeability, averaging, homogenization, periodic media, upscaling.

## Nomenclature

$\underline{e}$  ( $= -\nabla p$ ) fine-scale driving force vector per unit volume [ $\text{N m}^{-3}$ ].  
 $\tilde{e}_i$  ( $= -\partial p / \partial \xi_i = h_i e_i$ ) fine-scale pressure derivative [ $\text{Pa} (\text{unit}(\xi_i))^{-1}$ ].

$\underline{E}$	(= $-\nabla P$ ) upscaled (coarse-scale) driving force vector per unit volume [ $\text{N m}^{-3}$ ].
$\underline{\tilde{E}}_i$	(= $-\partial P/\partial \xi_i = h_i E_i$ upscaled (coarse-scale) pressure derivative [ $\text{Pa (unit}(\xi_i))^{-1}$ ].
$h_i$	( $i = 1, 2, 3$ ) scale factor in orthogonal curvilinear coordinate system [ $\text{m (unit}(\xi_i))^{-1}$ ].
$\underline{k}$	(= absolute permeability/dynamic viscosity) fine-scale mobility tensor [ $\text{m}^2 \text{Pa}^{-1} \text{s}^{-1}$ ].
$\underline{K}$	(= absolute permeability/dynamic viscosity) upscaled mobility tensor [ $\text{m}^2 \text{Pa}^{-1} \text{s}^{-1}$ ].
$p$	(= fluid pressure minus hydrostatic pressure) fine-scale reduced pressure [ $\text{Pa}$ ].
$P$	(= fluid pressure minus hydrostatic pressure) upscaled reduced pressure [ $\text{Pa}$ ].
$\underline{q}$	fine-scale flux density vector [ $\text{m s}^{-1}$ ].
$\underline{Q}$	upscaled flux density vector [ $\text{m s}^{-1}$ ].
$\underline{R}$	(= $\underline{K}^{-1}$ ) upscaled resistivity tensor [ $\text{Pa s m}^{-2}$ ].
$\underline{S}$	= either $\underline{K}$ or $\underline{R}$
$t$	time [s].
$\underline{x}$	position vector [m].

*Greek symbols*

$\phi$	(= $\underline{e} \cdot \underline{q}$ = linear combination of $\phi_{ij}$ ) fine-scale dissipation per unit volume [ $\text{W m}^{-3}$ ].
$\Phi$	(= $\underline{E} \cdot \underline{Q}$ = linear combination of $\Phi_{ij}$ ) upscaled dissipation per unit volume [ $\text{W m}^{-3}$ ].
$\phi_{ij}$	(= $\underline{e}_i \cdot \underline{q}_j$ , $i, j = 1, 2, 3$ ) component of fine-scale dissipation per unit volume [ $\text{W m}^{-3}$ ].
$\Phi_{ij}$	(= $\underline{E}_i \cdot \underline{Q}_j$ , $i, j = 1, 2, 3$ ) component of upscaled dissipation per unit volume [ $\text{W m}^{-3}$ ].
$\xi_i$	( $i = 1, 2, 3$ ) orthogonal curvilinear coordinate [ $\text{m (unit}(h_i))^{-1}$ ].

## 1. Introduction

The modeling of hydrocarbon reservoirs by reservoir engineers, and of aquifer-aquitard systems by geohydrologists, has traditionally been separated into two activities: geological modeling and fluid flow modeling. These two modeling activities reflect different aspects of the same part of the subsurface that is studied, the rocks and the fluids contained in them. The geological model highlights the structural elements of the subsurface, the geometry and dimensions of its layers and faults, together with its rock types and properties. The fluid flow model is set up in terms of dynamic flow quantities like pressure, flux and dissipation. These quantities are related to each other by rock parameters like permeability, storage coefficient, porosity and capillary pressure. Since the ultimate goal of the two models is decision-making with respect to the same particular part of the subsurface – for instance to optimally and safely exploit a hydrocarbon reservoir, or a fresh water aquifer - the two models have to be matched. However, when trying to match the geological and the fluid flow model, it generally turns out that the spatial scales of the two models differ. As an example, the geological reservoir model may be built from units of meters in length and width and less than a meter in thickness, whereas the fluid flow model is built from units that are at least a hundred times larger in volume.

One approach to counter this mismatch in spatial scales is to make the scale of the fluid flow model finer. This 'multi-million-grid-cell' approach will be made feasible by the next generation of multi-processor computers. However, there will

always be a need to run fluid flow problems on relatively simple and cheap computers like PCs. In this way quick and user-friendly assessments can be made, even with run times that are so fast that simulations can be done in parallel with real-time measurements. For this approach the spatial scale of the geological model has to be made much coarser than for the multi-million-grid-cell approach. Therefore, the fine-scale rock properties, say the fine-scale permeabilities, of the geological data model have to be ‘upscaled’ to coarse-scale properties, the upscaled permeabilities, that can relate spatially averaged flow quantities, like averaged pressure, pressure derivatives, flux and dissipation. The upscaled parameters, e.g. upscaled permeabilities, are themselves not simple averages. Instead they have to be derived from the spatially averaged flow quantities, in such a way that well-known physical laws on the fine scale, like Darcy’s law or Onsager’s thermodynamic laws, remain valid as much as possible on the coarse scale.

An important consequence of upscaling is the emergence of anisotropy. Even if the heterogeneous fine-scale permeability  $k(x, y, z)$  is isotropic, the upscaled permeability is a tensor  $\underline{K}$ . In a coordinate system, this tensor is represented by its matrix of components

$$\begin{pmatrix} K_{xx} & K_{xy} & K_{xz} \\ K_{yx} & K_{yy} & K_{yz} \\ K_{zx} & K_{zy} & K_{zz} \end{pmatrix}.$$

Unfortunately, many finite difference programs for the simulation of fluid flow in reservoirs or aquifer-aquitard systems lack the possibility of handling the off-diagonal components in the above matrix. This diminishes the motivation to correctly compute upscaled permeabilities. However, in principle, methods exist to cope with off-diagonal permeability components in finite difference methods (Aavatsmark *et al.*, 1996).

In this paper we consider single-phase flow of a fluid with constant viscosity and density. In that case the absolute permeability and the storage coefficient are the two relevant parameters that couple the geological model with the fluid flow model. Here we focus on the absolute permeability tensor, since this is the most dominant parameter affecting fluid flow, while it is also the most heterogeneous parameter. Mathematical theories for the upscaling, especially homogenization theory for the upscaling of periodic media, are well-established (Bensoussan *et al.*, 1978; Sanchez-Palencia, 1980; Auriault, 1983; Quintard and Whitaker, 1988; Panfilov, 1992; Bøe, 1994; Hornung, 1997). Here, the upscaling and homogenization theory will be summarized from a physical point of view, aiming at understanding rather than mathematical rigorousness. Since the resulting equations are too complex to be solved analytically, numerical finite element approximations will be presented. To assess the accuracy of the numerical approximations, the conventional conformal-nodal finite element method will be used as an upper bound method, while the mixed-hybrid finite element method will be applied as a lower bound method.

In Section 2, the notion of ‘spatial averaging’ of the flow quantities pressure minus hydrostatic pressure (briefly pressure), pressure derivatives with respect to curvilinear coordinates (briefly pressure derivatives), flux density (briefly flux) and dissipation per unit volume (briefly dissipation) is defined for general upscaling volumes. The averaging operator is defined in such a way that the derivatives of the averaged pressure are equal to the average of the pressure derivatives. For upscaling domains with the shape of a rectangular parallelepiped this definition leads to the well-known volume-averaging operator. On the other hand, for cylindrical upscaling domains around a well, this definition leads to a spatial averaging operator that is different from volume averaging.

After having defined the averaging operator, this operator is used to introduce three requirements for upscaling. These three requirements such that the continuity equation and the dissipation equation, which is related to Onsager’s reciprocal thermodynamic relations, remain valid (are ‘conserved’) on the coarse scale.

In Section 3, three approaches to upscaling are presented: pressure–flux averaging (PF), pressure–dissipation averaging (PD) and flux–dissipation averaging (FD). These three approaches are such that Darcy’s law remains valid (is ‘conserved’) on the coarse scale. In general the three upscaled permeabilities obtained by these three approaches differ from each other. It is, however, advised to choose the coarse-scale grid system, for which the upscaling is applied, in such a way that the differences between the three upscaling approaches are minimized. This can be done by looking for periodic or nearly periodic subdomains of the subsurface (Section 4). Arguments in favor of each of the three upscaling approaches are briefly summarized.

In Section 4 the physics of homogenization is presented. Homogenization is an approach to upscaling that can be used for periodic porous media. In the literature, the theory of homogenization is generally presented from a mathematical point of view based on multi-scale asymptotic analysis (Bensoussan *et al.*, 1978; Sanchez-Palencia, 1980; Hornung, 1997). In contrast to this mathematical rigorousness, a relatively simple physical presentation of the upscaling and homogenization theory is presented here, aiming at insight and leaving away the mathematical intricacies. It is shown that the three different PF, PD and FD averaging approaches to upscaling, as presented in Section 3, yield exactly the same coarse-scale permeability for periodic porous media. Only in numerical approximations the three different algorithms for the three averaging approaches may yield slightly different results because of numerical errors.

The spatial fine-scale distribution of the absolute permeability is generally so intricate that exact solutions of the homogenized permeability cannot be found. Therefore, numerical approximation methods have to be applied. In Section 5 both the conformal-nodal finite element method (CN-FEM) and the mixed-hybrid finite element method (MH-FEM) are briefly introduced, especially with regard to their upper and lower bound properties.

In Section 6, three numerical examples are presented. The first example deals with a two-dimensional (2D) isotropic fine-scale permeability distribution that is just on the percolation threshold. Since an exact solution is available, the numerical methods can be validated and the importance of local grid refinement near the singular permeability points will be shown. The second example deals with a three-dimensional (3D) anisotropic fine-scale permeability distribution. Also here the exact upscaled permeability matrix is known. Since this permeability distribution is not piece-wise constant, but continuous, apparent deviations from the upper/lower bound theory will be observed. The third example deals with a field case in which a relatively high aspect ratio of the homogenization domain is present. In this case slight numerical differences between the PF and PD averaging approach become visible.

Finally, in Section 7 the results and conclusions are presented.

## 2. Three Requirements for Upscaling

Let us first consider the flow quantities like pressure, flux, etc. in an orthogonal curvilinear coordinate system with coordinates  $\xi_1, \xi_2, \xi_3$  and scale factors  $h_1, h_2, h_3$  (Morse and Feshbach, 1953, pp. 44–54). In many applications the upscaling volumes may simply be considered as rectangular parallelepipeds and then Cartesian coordinates  $\xi_1 = x, \xi_2 = y, \xi_3 = z$  suffice. However, near areas of special interest, like fractured regions, faults and wells, general curvilinear coordinates are often more appropriate.

Preferably, procedures for upscaling of the absolute permeability should satisfy three requirements.

### 2.1. REQUIREMENT (i): ‘CONSERVATION’ OF DRIVING FORCE

The upscaled pressure  $P(\xi_1, \xi_2, \xi_3)$  should be equal to a spatial average  $\langle p \rangle(\xi_1, \xi_2, \xi_3)$  of the fine-scale pressure  $p(\xi_1, \xi_2, \xi_3)$  while, at the same time, the upscaled pressure derivative  $\tilde{E}_i = -\partial P / \partial \xi_i$  should be equal to the average pressure derivative  $\langle \tilde{e}_i \rangle = -\langle \partial p / \partial \xi_i \rangle$ . When this requirement is satisfied, both the upscaled pressure and its spatial derivatives with respect to the coordinates have a similar well-defined meaning, respectively a pressure average and a driving force average. A spatial averaging operator  $\langle \cdot \rangle$  that is consistent with this requirement is given by

$$\begin{aligned} \langle f \rangle(\xi_1, \xi_2, \xi_3) &= \frac{1}{\Delta \xi_1 \Delta \xi_2, \Delta \xi_3} \times \\ &\times \int_{\xi_1 - \frac{1}{2} \Delta \xi_1}^{\xi_1 + \frac{1}{2} \Delta \xi_1} \int_{\xi_2 - \frac{1}{2} \Delta \xi_2}^{\xi_2 + \frac{1}{2} \Delta \xi_2} \int_{\xi_3 - \frac{1}{2} \Delta \xi_3}^{\xi_3 + \frac{1}{2} \Delta \xi_3} f(\xi_1^j, \xi_2^j, \xi_3^j) d\xi_1^j d\xi_2^j d\xi_3^j. \end{aligned} \quad (1)$$

Due to the factor 1/2 in the upper and lower bound of the integrals,  $\langle \xi_i \rangle = \xi_i, i = 1, 2, 3$ . The volume-averaging operator  $\langle \cdot \rangle_V$  is related to the above spatial operator

by  $\langle f \rangle_V = (V^{(\xi)}/V)\langle f h_1 h_2 h_3 \rangle$ , where

$$V^{(\xi)} = \Delta\xi_1 \Delta\xi_2 \Delta\xi_3 \quad \text{and} \quad V = \iiint_D h_1 h_2 h_3 \, d\xi_1 \, d\xi_2 \, d\xi_3$$

is the volume of the upscaling domain. When the upscaling domain is a rectangular parallelepiped, Cartesian coordinates, with  $h_1 = h_2 = h_3 = 1$ , are appropriate. Then the spatial averaging operator  $\langle \cdot \rangle$  means volume averaging. However, around wells, where the circular cylinder coordinates  $\xi_1 = r$ ,  $\xi_2 = \varphi$ ,  $\xi_3 = z$ , with  $h_2 = r$ ,  $h_1 = h_3 = 1$ , are the proper choice, the averaging operator  $\langle \cdot \rangle$  in Equation (1) differs from volume averaging.

## 2.2. REQUIREMENT (ii): ‘CONSERVATION’ OF CONTINUITY EQUATION

The second requirement is that the upscaled flux components times upscaled factors,  $Q_i H_1 H_2 H_3 / H_i$ , should be equal to the spatially averaged flux components times scale factors  $\langle q_i h_1 h_2 h_3 / h_i \rangle$  ( $i = 1, 2, 3$ , no summation over index  $i$ ). For Cartesian coordinates, the scale factors are  $h_1 = h_2 = h_3 = 1$  and the upscaled factors are also  $H_1 = H_2 = H_3 = 1$ . However, for circular cylinder coordinates, where  $h_2 = r$ ,  $h_1 = h_3 = 1$ , upscaled factor values  $H_2 = r$ ,  $H_1 = H_3 = 1$  are a good approximation only for not too large upscaling domains. The exact determination of the upscaled factors will not be discussed in this paper. When requirement (ii) is satisfied, the continuity equation for the upscaled flux is the same as the steady-state continuity equation for the fine-scale flux,  $\nabla \cdot \underline{q} = 0$  (Section 5), since, according to Equation (1)

$$\begin{aligned} \langle h_1 h_2 h_3 \nabla \cdot \underline{q} \rangle &= \left\langle \sum_{i=1}^3 \frac{\partial}{\partial \xi_i} \left( \frac{q_i h_1 h_2 h_3}{h_i} \right) \right\rangle = \sum_{i=1}^3 \frac{\partial}{\partial \xi_i} \left\langle \frac{q_i h_1 h_2 h_3}{h_i} \right\rangle \\ &= \sum_{i=1}^3 \frac{\partial}{\partial \xi_i} \left( \frac{Q_i H_1 H_2 H_3}{H_i} \right). \end{aligned}$$

(Morse and Feshbach, 1953, pp. 115–116). This way the upscaled flux has a well-defined meaning of spatial flux average, similar to the meanings of the upscaled pressure and the upscaled pressure derivatives in requirement (i). Especially in transport problems, where the flow velocity plays a dominant role, requirement (ii) will be important.

## 2.3. REQUIREMENT (iii): ‘CONSERVATION’ OF DISSIPATION EQUATION

The third requirement is that the upscaled dissipation (per unit volume)

$$\Phi = \frac{V^{(\xi)}}{V} \sum_{i=1}^3 \frac{\tilde{E}_i Q_i H_1 H_2 H_3}{H_i}$$

should be equal to the volume average of the fine-scale dissipation

$$\langle \phi \rangle_V = \langle -\nabla p \cdot \underline{q} \rangle_V = \frac{V^{(\xi)}}{V} \sum_{i=1}^3 \left\langle \frac{\tilde{e}_i q_i h_1 h_2 h_3}{h_i} \right\rangle.$$

This requirement expresses that on the coarse scale the dissipation equation is equal to that on the fine scale. This is sometimes called ‘conservation of dissipation’ (Bøe, 1994). The dissipation per unit volume is the rate of irreversible conversion of mechanical energy to internal energy within the upscaling domain, divided by the volume of the upscaling domain. From a microscopic point of view, the irreversible conversion rate is caused by the viscous shear stresses that are associated with the Stokes flow in the pore space. If requirement (iii) is satisfied, thermodynamic equations of the upscaled flow, entropy production, Onsager’s reciprocal relations, etc., have the same form as the thermodynamic equations describing the fine-scale thermodynamics (Case, 1994, pp. 202–205).

Unfortunately, in general porous media the above three requirements over-specify the upscaling problem. However, both perfectly layered porous media and periodic porous media can be upscaled in such a way that the three requirements are satisfied simultaneously. Upscaling of perfectly porous media is almost trivial (Zijl and Nawalany, 1993, pp. 71–74), therefore this paper will concentrate on upscaling of periodic media.

### 3. Three Approaches to Upscaling ‘Conserving’ Darcy’s Law

From now on only upscaling related to volume averaging will be considered. In that case the scale factors do no longer play role. They are equal to one, which means that  $e_i = \tilde{e}_i$ ,  $E_i = \tilde{E}_i$ ,  $\underline{e} = -\nabla p$  and  $\underline{E} = -\nabla P$ . As has been shown in Section 2, volume averaging excludes upscaling over domains near areas of special interest, like fractured regions, faults and wells, where curvilinear coordinate planes bound the upscaling domain. Since, in general, only two of the three upscaling requirements mentioned in Section 1 can be satisfied simultaneously, upscaling based on volume averaging can be performed in three ways:

1. *Pressure–Flux averaging (PF)*: The pressure–flux (PF) averaging approach to upscaling combines requirements (i) and (ii) of Section 2 using  $\langle \underline{q}_i \rangle = \underline{\underline{K}}_{\text{PF}} \cdot \langle \underline{e}_i \rangle$  to determine the upscaled mobility  $\underline{\underline{K}}_{\text{PF}}$ .
2. *Pressure–Dissipation averaging (PD)*: The pressure–dissipation (PD) averaging approach to upscaling combines requirements (i) and (iii) of Section 2 using  $\langle \underline{e}_i \rangle \cdot \underline{\underline{K}}_{\text{PD}} \cdot \langle \underline{e}_j \rangle = \langle \phi_{ij} \rangle$  to determine the upscaled mobility  $\underline{\underline{K}}_{\text{PD}}$ , where  $\phi_{ij} = \underline{e}_i \cdot \underline{q}_j$  is a component of the fine-scale dissipation matrix.
3. *Flux–Dissipation averaging (FD)*: The flux–dissipation (FD) averaging approach to upscaling combines requirements (ii) and (iii) of Section 2 using  $\langle \underline{q}_j \rangle \cdot \underline{\underline{K}}_{\text{FD}}^{-1} \cdot \langle \underline{q}_i \rangle = \langle \phi_{ij} \rangle$  to determine the upscaled mobility  $\underline{\underline{K}}_{\text{FD}}$ .

The three thus-determined upscaled mobilities are not independent; they are related to each other by the expression  $\underline{\underline{K}}_{\text{FD}}^{-1} = \underline{\underline{K}}_{\text{PF}}^{-T} \cdot \underline{\underline{K}}_{\text{PD}} \cdot \underline{\underline{K}}_{\text{PF}}^{-1}$ . Because of this dependence, we will from now on focus on the pressure–flux and the pressure–dissipation averaging approach only.

Since the fine-scale mobility tensor  $\underline{k}$  is symmetric ( $\underline{k} = \underline{k}^T$ ) and positive definite (King *et al.*, 1995), it follows from the above-given definitions that also  $\underline{\underline{K}}_{\text{PD}} = \underline{\underline{K}}_{\text{PD}}^T$  and  $\underline{\underline{K}}_{\text{FD}} = \underline{\underline{K}}_{\text{FD}}^T$  are symmetric and positive definite. However, in general,  $\underline{\underline{K}}_{\text{PF}} \neq \underline{\underline{K}}_{\text{PF}}^T$  is non-symmetric (Zijl and Nawalany, 1993, pp. 85–89; Bentzen, 1994; King *et al.*, 1995). Moreover, there is no a priori guarantee that  $\underline{\underline{K}}_{\text{PF}}$  is positive definite. These ‘poor’ properties of the upscaled mobility tensor may be considered as a serious disadvantage of the PF averaging approach. It is sometimes even claimed that non-symmetric mobility tensors have no physical meaning because of their complex eigenvalues, which cannot be interpreted as principal mobilities (Durlafsky, 1992). However, using a singular value decomposition instead of an eigenvalue decomposition, it can be shown that not only symmetric mobility tensors, but also non-symmetric mobility tensors have real principal mobilities with a physical meaning (Zijl and Nawalany, 1993, pp. 89–96). An advantage of the PF averaging approach is that the matrix of coarse-scale mobility components has nine independent elements, while the PD and FD averaging approach lead to only six independent elements. Hence, the PF averaged mobility tensor contains more information about the original fine-scale distribution than the PD and FD averaged mobility tensors.

If the porous medium is periodic, the upscaling can be performed by homogenization. This procedure will be explained in Section 4, where it will be proved that, for periodic porous media,  $\underline{\underline{K}}_{\text{PF}} = \underline{\underline{K}}_{\text{PD}} = \underline{\underline{K}}_{\text{FD}} = \underline{\underline{K}} = \underline{\underline{K}}^T$ . Since all three averaging approaches have their specific advantages, it is recommended to choose the coarse grid system, in which the upscaling is performed, in such a way that the differences between the three averaging approaches are minimized. This can be done by aligning the inter-cell boundaries in such a way that as much periodicity as possible is obtained within the upscaling domains.

#### 4. The Physics of Homogenization

In periodic porous media the fine-scale permeability has translation symmetry in three different directions. For such media the smallest possible upscaling domain is a parallelepiped with sides that represent the periodicity interval of the translation symmetry. Even if the porous medium is periodic, upscaling domains that are bound by curvilinear coordinate planes, for instance upscaling domains bound by cylindrical coordinate planes around wells, cannot be periodicity domains. Hence, not only the choice of volume averaging (Section 2), but also the limitation to periodic upscaling domains (i.e., parallelepipeds) has to be relaxed when dealing with upscaling around wells. Below we limit the discussion to periodic upscaling domains.

Homogenization is an upscaling method that has been developed especially for periodic media. In the literature the method of homogenization is generally derived starting from a mathematical point of view, in which the method of multi-scale asymptotic expansions play an important part (Bensoussan *et al.*, 1978; Sanchez-Palencia, 1980; Hornung, 1997). Below, homogenization will be explained in a much simpler way based on a physical point of view.

In periodic media the upscaled flux  $\underline{Q}$  and the upscaled mobility  $\underline{K}$  are constant. Then Darcy's law,  $\underline{Q} = \underline{K} \cdot \underline{E}$ , yields a constant  $\underline{E}$  too. Since  $\underline{E} = -\nabla P(\underline{x})$ , the upscaled pressure is linear in  $\underline{x}$ , that is,  $P(\underline{x}) = -\underline{E} \cdot \underline{x}$  (Appendix A, Section A.1). In addition, the fine-scale pressure  $p(\underline{x})$  is equal to the upscaled pressure plus a periodic 'correction'  $\chi(\underline{x})$  that has the same axes of periodicity as the fine-scale mobility  $\underline{k}(\underline{x})$ . This periodicity yields (Appendix A, Section A.1)

$$\underline{E} = \langle \underline{e} \rangle, P(\underline{x}) = \langle P \rangle(\underline{x}). \quad (2)$$

All the above-presented considerations are required to hold for both unsteady and steady flow.

The basis of the method of homogenization is to equate the fine-scale differential operator to the upscaled differential operator that describes the outflow minus the inflow of fluid in a volume element. This operator is the same for unsteady and steady flow. This way we find (Appendix A, Section A.2)

$$\nabla \cdot (\underline{K} \cdot P(\underline{x})) = \nabla \cdot (\underline{k}(\underline{x}) \cdot \nabla p(\underline{x})). \quad (3)$$

Substituting constant  $\underline{K}$  and linear  $P(\underline{x})$  into the left side of Equation (3) yields the steady flow equation

$$\nabla \cdot (\underline{k}(\underline{x}) \cdot \nabla p(\underline{x})) = 0. \quad (4)$$

The fact that in Equation (4) the time does not appear makes that the upscaled mobility is time-independent, as it should be from a practical point of view. However, this approach cannot explain the early-time and late-time phenomena that are observed in media with very large contrasts in mobility, like fissured porous media. For such media more advanced upscaling methods are required (Barenblatt *et al.*, 1990, pp. 34–44; Panfilov, 1992).

Equation (4) has to be solved numerically in a periodicity domain, with  $\chi(\underline{x}) = p(\underline{x}) + \underline{E} \cdot \underline{x}$  boundary-periodic, that is, with 'constant-jump' boundary condition  $\Delta p = -\underline{E} \cdot \Delta \underline{x}$  for the pressure  $p(\underline{x})$  (Appendix A, Section A.3). Multiplication of Equation (3) for  $p(\underline{x}) = p_i(\underline{x})$  and  $P(\underline{x}) = P_i(\underline{x})$  by a fine-scale pressure  $p_j(\underline{x})$ , applying Gauss's divergence theorem, and using the periodicity, yields (Appendix A, Section A.4)

$$\underline{Q}_i = \langle \underline{q}_i \rangle \Leftrightarrow \langle \underline{e}_i \rangle \cdot \underline{K} \cdot \langle \underline{e}_j \rangle = \langle \phi_{ij} \rangle, \quad (5)$$

where  $\langle \phi_{ij} \rangle = \langle \underline{e}_i \cdot \underline{q}_j \rangle$  (Appendix A, Section A.5).

Combination of Equations (2) and (5) proves that  $\Phi_{ij} = \underline{E}_i \cdot \underline{Q}_j = \langle \phi_{ij} \rangle$  and, hence, that the PF, PD and FD averaging approaches yield equivalent results.

As an example to determine  $K_{ij}$ , ‘constant-jump’ boundary pressures for Equation (4) are chosen in such a way that  $P_1 = x$ ,  $P_2 = y$  and  $P_3 = z$ , that is,  $(E_{1x}, E_{1y}, E_{1z}) = -(1, 0, 0)$ ,  $(E_{2x}, E_{2y}, E_{2z}) = -(0, 1, 0)$  and  $(E_{3x}, E_{3y}, E_{3z}) = -(0, 0, 1)$ . Substitution of this choice into Darcy’s law and Equation (5) yields very simple expressions for the homogenized mobility: PF averaging yields  $K_{ij} = -\langle q_{ji} \rangle$  and PD averaging yields  $K_{ij} = \langle \phi_{ij} \rangle$ . This example shows that Equation (4) has to be solved three times, for three independent sets of boundary conditions. Any other choice of the ‘constant-jump’ pressure boundary conditions leads to the same homogenized mobility, however, with more complex expressions for  $K_{ij}$ .

## 5. Upper and Lower Bounds of Finite Element Methods

In this chapter some properties of finite element methods are summarized without prove. If the fine-scale mobility tensor is positive definite and symmetric, then Equation (4) is equivalent with a variational formulation that minimizes the dissipation in the upscaling domain under some constrains at the boundaries of that domain. When finite element methods are applied to find an approximate solution, the approximated total dissipation is greater than (or equal to) the exact dissipation. In finite element methods, two ways of handling the boundary conditions can be distinguished. (A) exact specification of the ‘pressure jumps’  $\Delta p_i = -\Delta \underline{x} \cdot \underline{E}_i$  over the boundaries of the upscaling domain, and (B) approximate specification of the ‘pressure jumps’  $\Delta p_i = -\Delta \underline{x} \cdot \underline{K}^{-1} \cdot \underline{Q}_i$  over the boundaries of the upscaling domain. The essential difference is that in methods of type (A) the boundary conditions for the pressure are not subject to the numerical minimization procedure, while in methods of type (B) the boundary conditions are satisfied approximately, since they are part of the numerical minimization process.

It may be clarifying to mention the following correspondences. Since in type (A) methods  $\langle \underline{e}_i \rangle = \underline{E}_i$  is specified exactly, type (A) methods correspond in some way to the PD averaging approach. Similarly, since in type (B) methods  $\langle q_i \rangle = \underline{Q}_i$  is specified in such a way that it is not subject to the numerical minimization process, type (B) methods correspond in some way to the FD averaging approach. Roughly speaking, since finite element methods over estimate the dissipations  $\langle \underline{e}_i \rangle \cdot \underline{K} \cdot \langle \underline{e}_j \rangle = \langle \underline{q}_j \rangle \underline{K}^{-1} \cdot \langle \underline{q}_i \rangle = \langle \phi_{ij} \rangle$ , type (A) methods overestimate the homogenized mobility, while type (B) methods overestimate the inverse of the homogenized mobility, that is, they underestimate the homogenized mobility.

To be a bit more precise, it can be proved that in methods of type (A) the volume-averaged dissipation  $\langle \phi \rangle$  is proportional to the eigenvalues of  $\underline{K}$ , that is, proportional to the principal upscaled mobility components  $K_1, K_2, K_3$ . Similarly, in methods of type (B) the volume-averaged dissipation is proportional to the inverses of the eigenvalues, that is, proportional to the principal resistivities  $R_1 = K_1^{-1}, R_2 = K_2^{-1}, R_3 = K_3^{-1}$ . It follows then that finite element methods

of type (A) yield too large approximations for the principal components of the homogenized mobility (Duvaut and Lions, 1976, p. 64). On the other hand, methods of type (B), yield too small approximations for the principal components of the homogenized mobility (Penman, 1988). The conformal-nodal finite element method (CN-FEM) is of type (A), while the mixed-hybrid finite element method (MH-FEM) is of type (B).

From the fact that CN-FEM approximations yield principal mobilities that are too large, while MH-FEM approximations yield principal mobilities that are too small, it follows that principal mobilities can be used to assess error estimates for the accuracy of the numerical approximations. However, it will be more practical to avoid eigenvalue calculations. Therefore, error bounds will be assessed from the mobility components  $K_{ij}$  in the chosen coordinate system. From the upper and lower bound properties of the principal mobilities it follows that the sum of the numerically approximated diagonal mobilities  $\sum_{i=1}^3 K_{ii} = K_{xx} + K_{yy} + K_{zz}$  is too large for CN-FEM and too small for MH-FEM (Appendix B). This property can be used as a ‘hard’ error estimate.

Moreover, under the condition that the eigenvectors of  $\underline{K}$  are approximated sufficiently accurate (the preferential flow directions are calculated with sufficient accuracy), it can be proved that the individual diagonal mobilities  $K_{xx}$ ,  $K_{yy}$ , and  $K_{zz}$  are too large for CN-FEM and too small for MH-FEM (Appendix B). This property can be used as a ‘soft’ error estimate. When deviations from the ‘soft’ estimate are observed in the numerical examples, we may conclude that the preferential flow directions are not calculated ‘sufficiently accurate’.

Ribeiro and Romeu (1997) have applied a similar approach to the accuracy of 2D upscaling problems. When comparing how fast their numerical results converge when refining the grid, they observed that the (conformal-nodal) finite element method yields an upper bound, while the block centered finite difference method and the mixed-hybrid finite element method yield a lower bound. In the numerical examples presented in Section 6, the same is observed, also for 3D upscaling.

## 6. Numerical Examples

Homogenization software based on both the conformal-nodal finite element method (CN-FEM) and the mixed-hybrid finite element method (MH-FEM, Kaasschieter and Huijben, 1992) has been developed. The software is coded in portable standard FORTRAN-77 and can be used both ‘stand alone’ and as callable subroutines in a reservoir simulator (Trykozko and Zijl, 1999). A number of validation tests have been run.

### 6.1. SYNTHETIC 2D EXAMPLE USING LOCAL GRID REFINEMENT

The 2D periodic fine-scale permeability pattern of this example is shown in Figure 1. The porous medium consists of two different rock types: type 1 has a

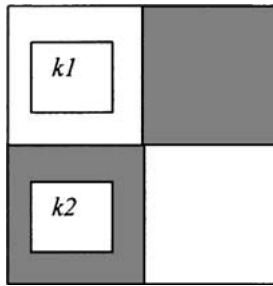


Figure 1. Periodic structure with singularities.

permeability of  $k_1 = 1$  mD, while the permeability of rock type 2 is 100 times smaller, that is,  $k_2 = 0.01$  mD.

For this case the exact homogenized permeability is known (Warren and Price, 1961)

$$K = K_{xx} = K_{yy} = \sqrt{k_1 k_2} \quad (\text{geometric mean}), \quad (6.1)$$

$$K_{xy} = K_{yx} = 0. \quad (6.2)$$

As far as the numerical approximations are concerned, large differences in the results obtained with the two methods CN-FEM and MH-FEM have been encountered. The values obtained with the CN-FEM on the minimal admissible mesh consisting of nine nodes are equal to the *arithmetic* mean, whereas the solution obtained with MH-FEM on the same mesh is equal to the *harmonic* mean.

This large difference between the two solutions is caused by the presence of the singularity points in the fine-scale mobility reflecting a situation just between disconnected and interconnected channels. One way of decreasing the influence of the singularities on the accuracy of the solution is to refine the computational mesh, thus making the domain of influence of the singularity smaller. Computations were performed for a sequence of uniformly refined meshes, of which the triangulation pattern of the mesh is shown in Figure 2. Figure 3 gives the homogenized values  $K = K_{xx} = K_{yy}$  obtained with the two numerical methods plotted as a function of the number of nodes. There is an improvement of the quality of the solution as the

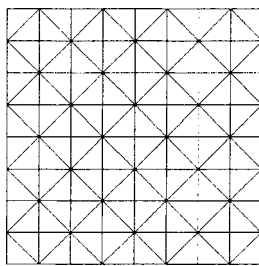


Figure 2. Uniform triangular FE mesh.

Upper and lower bounds

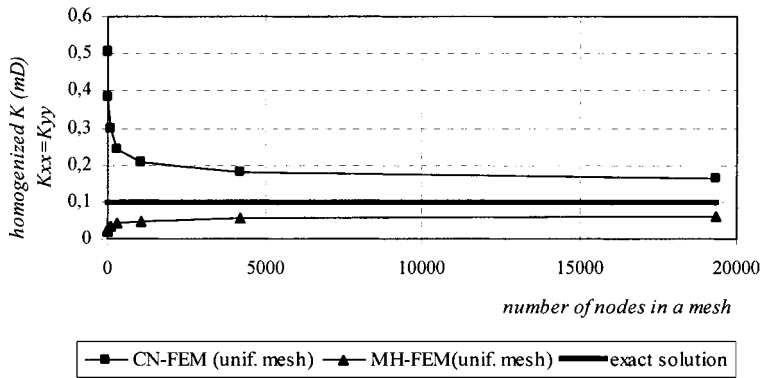


Figure 3. Upper and lower bounds for a sequence of uniform meshes.

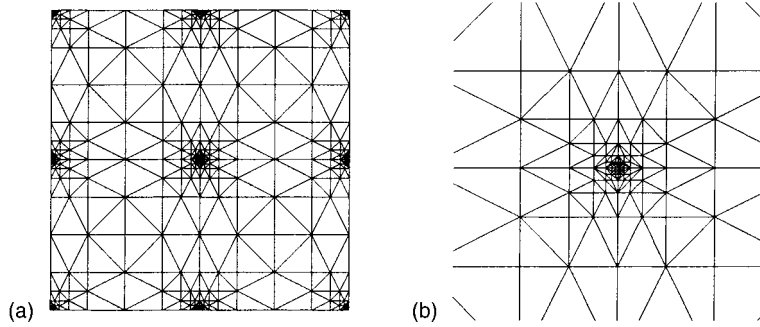


Figure 4. (a) Refinement around singularity points and (b) details of local grid refinement.

mesh is becoming finer, though the convergence is slow. Upper and lower bounds hold.

The next step was to apply a non-uniform refinement producing a very fine mesh only in the nearest vicinity of a singularity (Figure 4). The results are significantly better (Figure 5) and the convergence to the exact solution is faster than in the uniform case.

6.2. SYNTHETIC 3D EXAMPLE WITH CONTINUOUS FINE-SCALE MOBILITY

In this example, the applicability of the homogenization software to periodic porous media with off-diagonal fine-scale permeability components is demonstrated. Consider a periodic porous medium in which  $u$ ,  $v$  and  $w$  are the three orthogonal axes of translation symmetry. The artificial coordinate system, with axes  $x$ ,  $y$  and  $z$ , is chosen in such a way that  $x$  and  $y$  make an angle of 30 degrees with the ‘natural’  $u$  and  $v$  axes, while  $z = w$ . (We use dimensionless coordinates related to a char-

## Upper and lower bounds

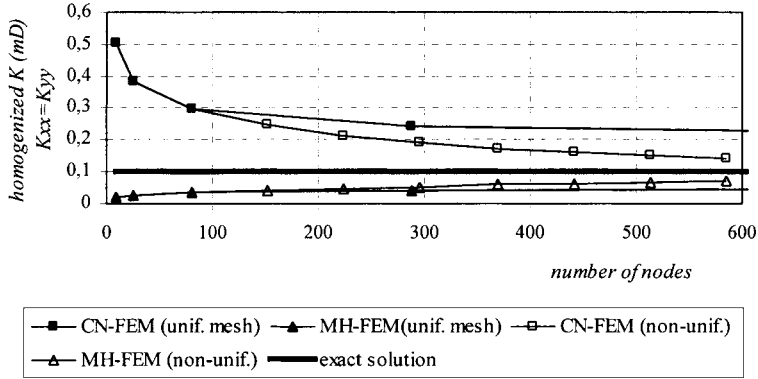


Figure 5. Upper and lower bounds for a sequence of non-uniform meshes.

acteristic length.) Hence, the following parameters define one single periodicity domain

$$\begin{aligned}
 -\frac{1}{2}\alpha &\leq u = \frac{1}{2}\sqrt{3}x - \frac{1}{2}y \leq \frac{1}{2}\alpha, \\
 -\frac{1}{2}\beta &\leq v = \frac{1}{2}x + \frac{1}{2}\sqrt{3}y \leq \frac{1}{2}\beta, \\
 -(1-\gamma) &\leq w = z \leq 1-\gamma.
 \end{aligned} \tag{7.1}$$

In expression (7.1)  $\alpha$ ,  $\beta$ , and  $\gamma$  are numerical values. In this example they are chosen as  $\alpha = \beta = 196/100$  and  $\gamma = 2/100$ .

The fine-scale permeability distribution within the above-given periodicity domain is given by

$$\begin{aligned}
 \begin{pmatrix} k_{xx} & k_{xy} & k_{xz} \\ k_{yx} & k_{yy} & k_{yz} \\ k_{zx} & k_{zy} & k_{zz} \end{pmatrix} &= \begin{pmatrix} \frac{31}{40} & -\frac{9}{40}\sqrt{3} & 0 \\ -\frac{9}{40}\sqrt{3} & \frac{13}{40} & 0 \\ 0 & 0 & \frac{1}{100} \end{pmatrix} \times \\
 &\times \cosh^2\left(\frac{1}{2}\sqrt{3}x - \frac{1}{2}y\right) \cosh^2\left(\frac{1}{2}x + \frac{1}{2}\sqrt{3}y\right) \cos^2\left(\frac{1}{2}\pi z\right).
 \end{aligned} \tag{7.2}$$

(We use dimensionless permeabilities related to a characteristic permeability.) Outside the periodicity domain given by expressions (7), the above fine-scale permeability distribution is continued periodically. The exact upscaled permeability is given

by (Zijl and Trykozko, 1999)

$$\begin{aligned}
 & \begin{pmatrix} K_{xx} & K_{xy} & K_{xz} \\ K_{yx} & K_{yy} & K_{yz} \\ K_{zx} & K_{zy} & K_{zz} \end{pmatrix} \\
 &= \begin{pmatrix} \frac{1}{4}(3F_{uu} + \frac{1}{10}F_{vv}) & -\frac{1}{4}\sqrt{3}(F_{uu} - \frac{1}{10}F_{vv}) & 0 \\ -\frac{1}{4}\sqrt{3}(F_{uu} - \frac{1}{10}F_{vv}) & \frac{1}{4}(F_{uu} + \frac{3}{10}F_{vv}) & 0 \\ 0 & 0 & \frac{1}{100}F_{zz} \end{pmatrix}, \quad (8.1)
 \end{aligned}$$

where

$$F_{uu} = \frac{1}{8} \frac{\alpha}{\beta(1-\gamma)\pi} \coth\left(\frac{1}{2}\alpha\right) (\beta + \sinh \beta)((1-\gamma)\pi + \sin(\pi\gamma)), \quad (8.2)$$

$$F_{vv} = \frac{1}{8} \frac{\beta}{\alpha(1-\gamma)\pi} \coth\left(\frac{1}{2}\beta\right) (\alpha + \sinh \alpha)((1-\gamma)\pi + \sin(\pi\gamma)), \quad (8.3)$$

$$F_{zz} = \frac{1}{8} \frac{(1-\gamma)\pi}{\alpha\beta} \tan\left(\frac{1}{2}\pi\gamma\right) (\alpha + \sinh \alpha)(\beta + \sinh \beta). \quad (8.4)$$

The 3D-mesh generation procedure consisted of two steps. First, the upscaling domain has been divided into hexahedra. The second step is the division of each hexahedron into 5 tetrahedra. Five different mesh sizes have been applied, based on a division into  $6 \times 6 \times 6$ ,  $10 \times 10 \times 10$ ,  $14 \times 14 \times 14$ ,  $20 \times 20 \times 20$  and  $30 \times 30 \times 30$  hexahedral cells. In Figures 6(a)–(e) the results are displayed.

It is observed that CN-FEM yields higher values for  $K_{xx} + K_{yy} + K_{zz}$  than MH-FEM, as it should be according to the theory. However, the exact solution is not in between the CN-FEM and MH-FEM solution. This seems to contradict the statement from Section 5 that CN-FEM gives an upper bound and MH-FEM gives a lower bound. However, this statement holds only if the fine-scale permeability is represented exactly in the numerical model. In this example, the continuous fine-scale permeability components cannot be represented exactly. They have to be approximated by a distribution of piecewise constant permeability components. Here the components are constant within each hexahedral cell, with constant values that have been chosen equal to the value of the continuous fine-scale permeability component at the center of the cell.

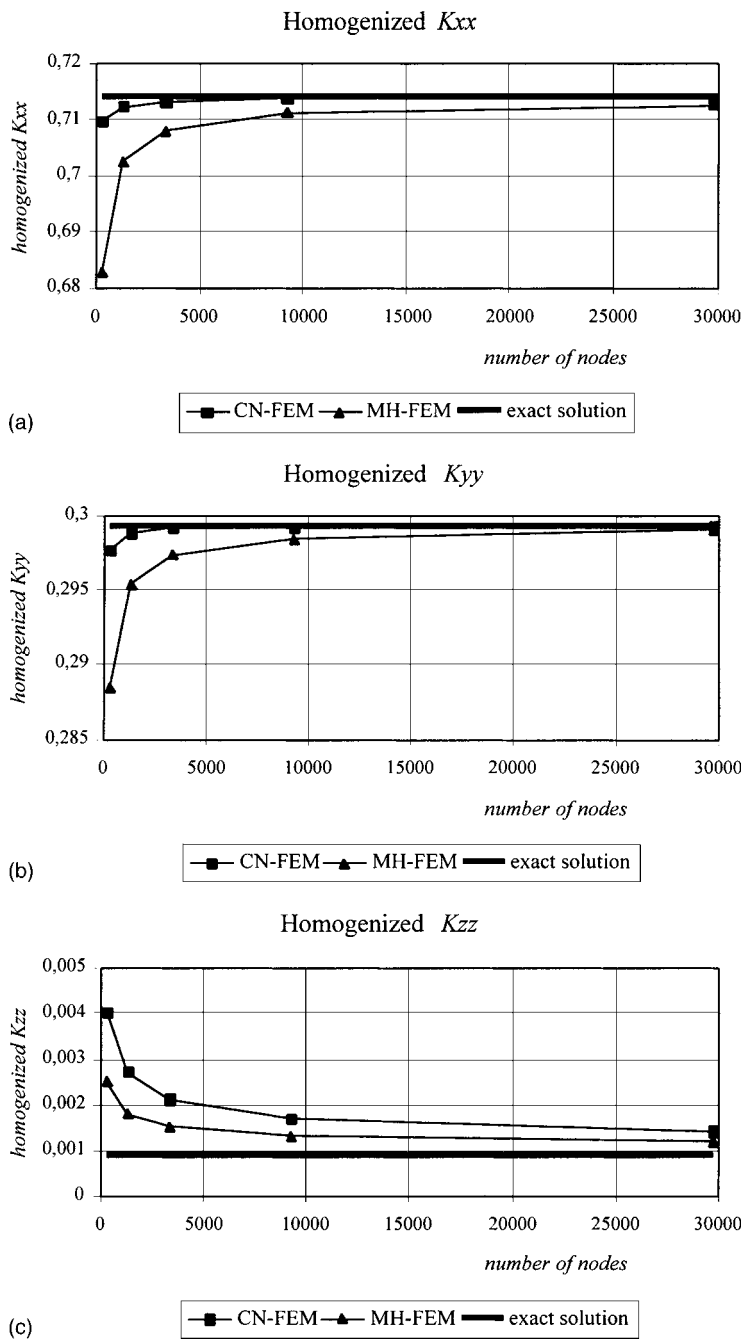


Figure 6. (a) Homogenized permeability  $K_{xx}$  for a sequence of refined meshes. (b) Homogenized permeability  $K_{yy}$  for a sequence of refined meshes. (c) Homogenized permeability  $K_{zz}$  for a sequence of refined meshes. (d) Homogenized permeability  $K_{xy} = K_{yx}$  for a sequence of refined meshes. (e) Trace  $K_{xx} + K_{yy} + K_{zz}$  of homogenized permeabilities for a sequence of refined meshes.

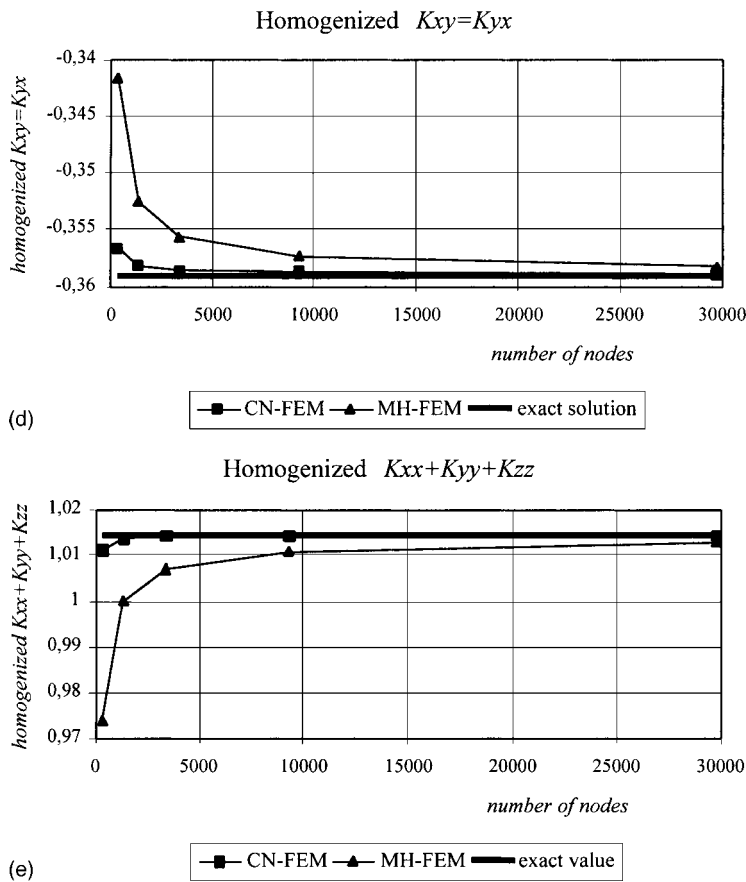


Figure 6. (continued)

### 6.3. FIELD EXAMPLE

In this field example, the isotropic fine-scale permeability varies from 213.188 mD to 13984.5 mD, cf. Figure 7. Originally, the upscaling domain has been divided into 384 hexahedral cells ( $6 \times 8 \times 8$ ). There are 26 'inactive' cells, which means

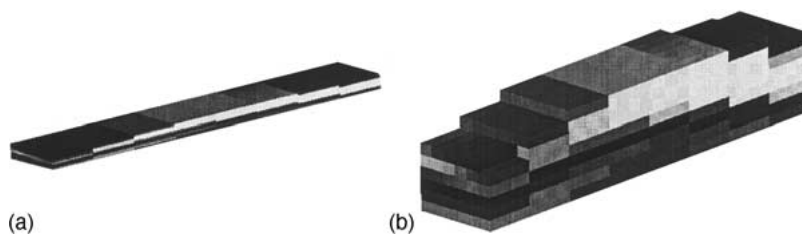


Figure 7. (a) Fine-scale permeability distribution. (b) Fine-scale permeability distribution with exaggerated vertical dimension; the inactive cells are omitted.

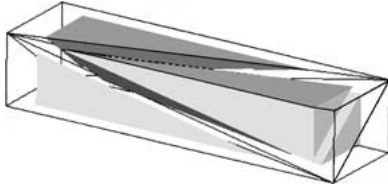


Figure 8. One hexahedral cell divided in five tetrahedra (exaggerated vertical dimension).

Table I. Original mesh

567 nodes, 1920 elements, 4160 interfaces
CN-FEM: 384 unknowns (nodal pressures)
MH-FEM: 3840 unknowns (interfacial normal fluxes)

that the small value  $k = 0.0001$  mD has been assigned to the cell's permeability. Each cell is divided into five tetrahedral finite elements (Figure 8).

The geometry of this example is very anisotropic; the aspect ratio  $x/z$  is equal to 6, while the aspect ratio  $y/z$  is equal to 25. The characteristics of the two finite element models and the computed upscaled permeabilities are given in the Tables I, IIa and IIb.

The original mesh has been uniformly refined twice; the characteristics of the two finite element models are given in the Tables III and IV and are summarized in the Figures 9(a)–(g).

From the above figures we observe that the upper and lower bound properties of respectively CN-FEM and MH-FEM are satisfied for the diagonal sum (the trace)  $K_{xx} + K_{yy} + K_{zz}$ , as is required by the 'hard' error estimate. In addition, the upper and lower bound properties hold for the individual diagonal components  $K_{xx}$ ,  $K_{yy}$ , and  $K_{zz}$  too. This may be interpreted as an indication that the principal directions, and hence the directions of the preferential flow paths, are calculated accurately.

Table IIa. Matrix  $K_{ij}$  calculated by CN-FEM [mD]

Pressure–Dissipation averaging (exact symmetry)	$0.7481195 \times 10^4$	$0.2824882 \times 10^3$ $0.7378196 \times 10^4$	$0.1608522 \times 10^2$ $-0.3967316 \times 10^2$ $0.2619069 \times 10^4$
Diagonal sum		$= K_{xx} + K_{yy} + K_{zz}$	$= 1.7478460 \times 10^4$
Pressure–Flux averaging (approximate symmetry)	$0.7481552 \times 10^4$ $0.2824910 \times 10^3$ $0.1608575 \times 10^2$	$0.2824714 \times 10^3$ $0.7378195 \times 10^4$ $-0.3967352 \times 10^2$	$0.1610208 \times 10^2$ $-0.3967317 \times 10^2$ $0.2619069 \times 10^4$
Diagonal sum		$= K_{xx} + K_{yy} + K_{zz}$	$= 1.5802161 \times 10^4$

Table IIIb. Matrix  $K_{ij}$  calculated by MH-FEM [mD]

Pressure–Dissipation averaging (exact symmetry)	$0.7147581 \times 10^4$	$0.5357514 \times 10^3$ $0.6957348 \times 10^4$	$0.2795474 \times 10^2$ $-0.3247279 \times 10^2$ $0.1696884 \times 10^4$
Diagonal sum		$= K_{xx} + K_{yy} + K_{zz}$	$= 1.5801813 \times 10^4$
Pressure–Flux averaging (approximate symmetry)	$0.7147934 \times 10^4$	$0.5357587 \times 10^3$ $0.6957345 \times 10^4$ $-0.3247307 \times 10^2$	$0.2795624 \times 10^2$ $-0.3247307 \times 10^2$ $0.1696882 \times 10^4$
Diagonal sum		$= K_{xx} + K_{yy} + K_{zz}$	$= 1.5802161 \times 10^4$

Table III. Mesh after first refinement

3757 nodes, 15360 elements, 32000 interfaces
CN-FEM: 3072 unknowns
MH-FEM: 30720 unknowns (10 times more than CN-FEM)

Table IV. Mesh after second refinement

27225 nodes, 122880 elements, 250880 interfaces.
CN-FEM: 24576 unknowns
MH-FEM: 245760 unknowns

#### 6.4. DISCUSSION OF NUMERICAL RESULTS

All numerical examples show results that do not contradict the theory. In particular, the examples demonstrate clearly that the pressure–flux (PF) averaging approach yields the same upscaled permeability as the pressure–dissipation (PD) averaging approach.

We have also performed a number of numerical experiments in which the boundary conditions for the function  $\chi$  were not periodic. In other words, we have done experiments in which the ‘pressure jump’ from one boundary to its opposite boundary was no longer constant. Such boundary conditions represent non-periodic porous media. Under such conditions it is observed that the upscaled permeability obtained by the pressure–flux averaging approach,  $\underline{\underline{K}}_{\text{PF}}$ , becomes non-symmetric and, for sufficiently large deviations from periodic boundary conditions, the positive definiteness is lost too. On the other hand, the upscaled permeability obtained by the pressure–dissipation averaging approach,  $\underline{\underline{K}}_{\text{PD}}$ , remains

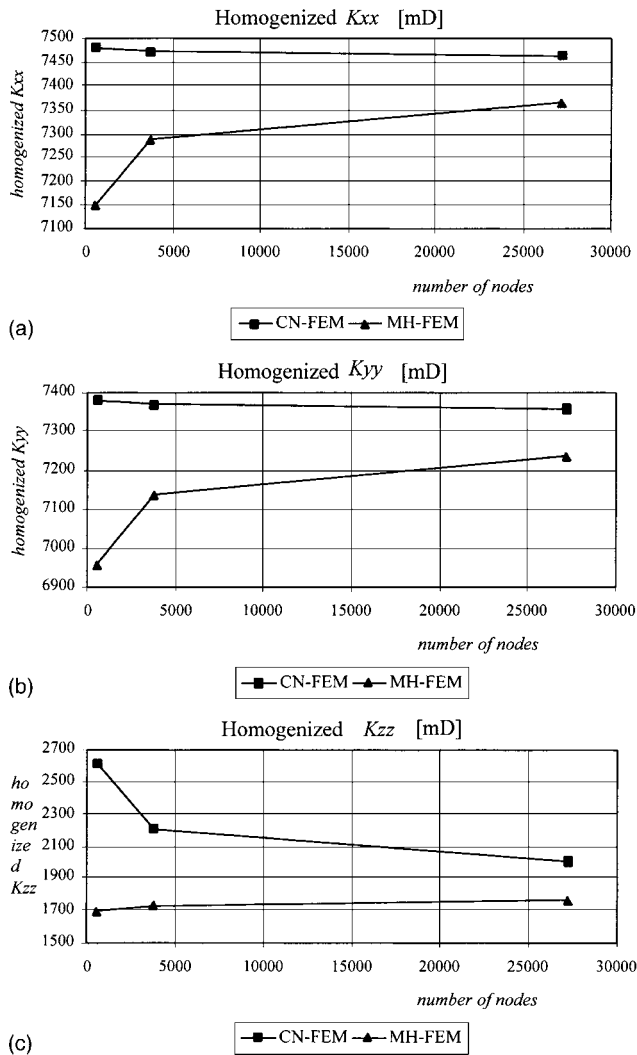
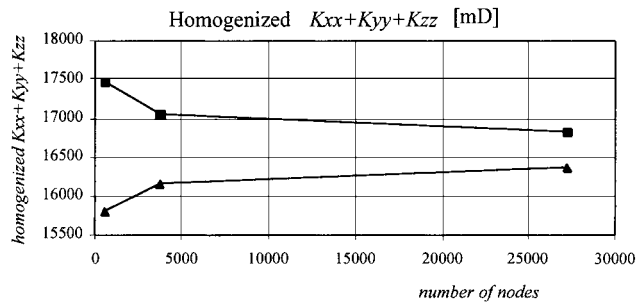


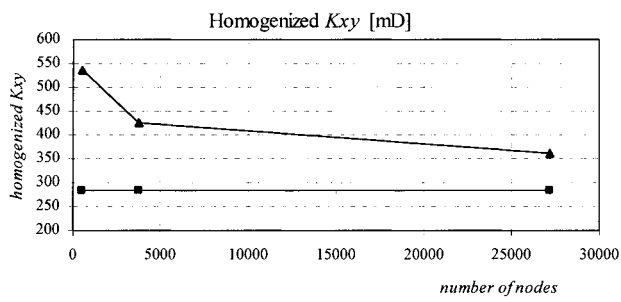
Figure 9. (a) Homogenized permeability  $K_{xx}$  for a sequence of refined meshes. (b) Homogenized permeability  $K_{yy}$  for a sequence of refined meshes. (c) Homogenized permeability  $K_{zz}$  for a sequence of refined meshes. (d) Trace  $K_{xx} + K_{yy} + K_{zz}$  of homogenized permeabilities for a sequence of refined meshes. (e) Homogenized permeability  $K_{xy}$  for a sequence of refined meshes. (f) Homogenized permeability  $K_{xz}$  for a sequence of refined meshes. (g) Homogenized permeability  $K_{yz}$  for a sequence of refined meshes.

symmetric and positive definite. This may be considered as an argument in favor of the pressure–dissipation averaging approach.

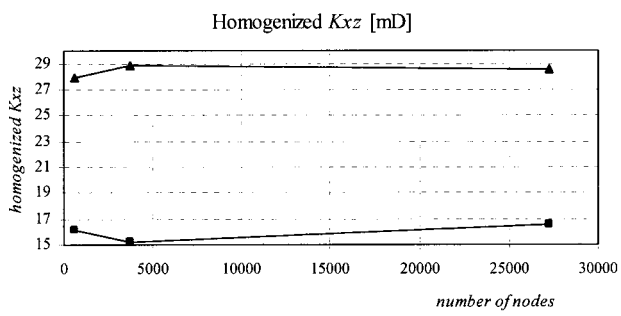
When performing the upscaling for domains with a homogeneous fine-scale permeability, the pressure–flux averaging approach yields always exactly the same homogeneous upscaled permeability, as expected. However, under non-periodic boundary conditions, the pressure–dissipation averaging approach yields an up-



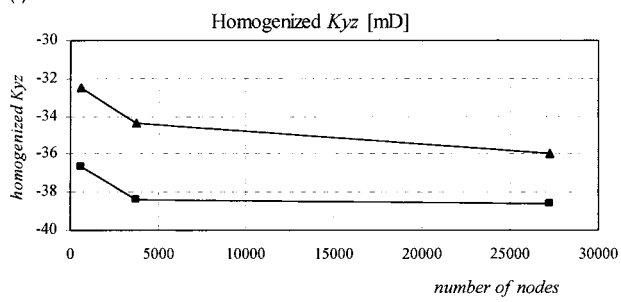
(d)



(e)



(f)



(g)

Figure 9. (continued)

scaled permeability that differs from the homogeneous fine-scale permeability. This may be considered as ‘non-physical’. This fact may be interpreted as a warning against the indiscriminate use of the pressure–dissipation averaging approach for non-periodic media. On the other hand, because of its relationship with variational methods, which minimize the dissipation functional (Section 5), the pressure–dissipation approach has many mathematical advantages, among which the possibility to use it in combination with multi-grid methods (Knapek, 1998).

## 7. Discussion and Conclusions

The modeling of hydrocarbon reservoirs and of aquifer-aquitard systems can be separated into two activities: geological modeling and fluid flow modeling. The geological model focuses on the geometry and the dimensions of the subsurface layers and faults, and on its rock types. The fluid flow model focuses on quantities like pressure, flux and dissipation, which are related to each other by the rock parameters permeability, storage coefficient, porosity and capillary pressure. The absolute permeability, which is the relevant parameter for steady single-phase flow of a fluid with constant viscosity and density, is studied here. When trying to match the geological model with the fluid flow model, it generally turns out that the spatial scale of the fluid flow model is built from units that are at least a hundred times larger in volume than the units of the geological model. To counter this mismatch in scales, the fine-scale permeabilities of the geological data model have to be ‘up-scaled’ to coarse-scale permeabilities that relate the average pressure, the average flux and the average dissipation to each other. The upscaled permeabilities are not simply averages. They are derived from the averaged flow quantities in such a way that the continuity equation, Darcy’s law and the dissipation equation remain valid on the coarse scale as much as possible.

In this paper the theory of upscaling has been presented from a physical point of view aiming at understanding, rather than mathematical rigorousness. Under the simplifying assumption of spatial periodicity of the fine-scale permeability distributions, homogenization theory can be applied. However, even under this assumption the spatial distribution of the permeability is generally so intricate that exact solutions of the homogenized permeability cannot be found.

Therefore, *numerical approximation* methods have been applied. To be able to estimate the approximation error, two numerical methods have been developed: one based on the conventional nodal finite element method (CN-FEM) and the other based on the mixed-hybrid finite element method (MH-FEM). CN-FEM gives an upper bound for the sum of the diagonal components of the homogenized mobility matrix, while MH-FEM gives a lower bound. Software for the numerical homogenization of 3D spatial distributions of the absolute permeability has been developed and tested. The software is coded in portable FORTRAN-77 and can be used as both ‘stand alone’ and as callable subroutines in reservoir simulators and groundwater flow models. The codes have been validated extensively by a number

of synthetic and field-data tests. Moreover, the two numerical approximation methods, CN-FEM and MH-FEM have been applied to three examples to estimate the numerical error as a function of the mesh density.

The upscaling described in this paper is based on the periodicity assumption. However, the theory presented in this paper can be extended. It has been identified how an extension to *upscaling without the periodicity assumption* has to be performed. Especially near areas of special interest, like fractured regions, faults and wells, such extensions will be important. To make such extensions possible, we have investigated two approaches: the pressure–flux (PF) averaging approach and the pressure–dissipation (PD) averaging approach. Under the periodicity assumption these two approaches yield the same upscaled permeability. However, for deviations from the periodicity assumption the two methods give different results. Some advantages and disadvantages of the two approaches are presented.

### Acknowledgements

Norsk Hydro has sponsored this work. The inspiring discussions with Dr. I. Aavatsmark and C. F. Eek-Jensen are greatly acknowledged.

### Appendix A

#### A.1. DRIVING FORCE

The fine-scale pressure is written as

$$p(\underline{x}) = c - \underline{E} \cdot \underline{x} + \chi(\underline{x}), \quad (\text{A.1})$$

where  $c$  is a constant. Taking the gradient yields

$$\underline{e}(\underline{x}) = -\nabla p(\underline{x}) = \underline{E} - \nabla \chi(\underline{x}). \quad (\text{A.2})$$

Integrating over the volume of the periodicity domain yields

$$\iiint_D \underline{e}(\underline{x}) \, dV = \underline{E} V - \iiint_D \nabla \chi(\underline{x}) \, dV. \quad (\text{A.3})$$

Since  $\chi(\underline{x})$  is a periodic function, the volume-average of its gradient is equal to zero. Hence

$$\underline{E} = \frac{1}{V} \iiint_D \underline{e}(\underline{x}) \, dV = \langle \underline{e} \rangle, \quad (\text{A.4})$$

which proves that the homogenized driving force is equal to the volume average of the fine-scale driving force.

## A.2. THE BASIC APPROACH TO HOMOGENIZATION

Homogenization is based on the following requirement

$$\nabla \cdot \underline{Q} = \nabla \cdot \underline{q}. \quad (\text{A.5})$$

Since the right-hand side of Equation (A.5) represents the outflow minus the inflow of a volume element, this equation requires that the homogenized flux represents the same outflow minus inflow. Equation (A.5) can be applied in two different ways.

## A.3. FIRST APPLICATION OF BASIC REQUIREMENT

Substituting constant  $\underline{Q}$  into the left-hand side of Equation (A.5) yields

$$\nabla \cdot \underline{q} = \nabla \cdot (\underline{k}(\underline{x}) \cdot \nabla p(\underline{x})) = 0. \quad (\text{A.6})$$

Equation (A.6) has to be solved in at least one periodicity domain with periodic boundary conditions for the function  $\chi(\underline{x})$ , that is, with constant ‘pressure jumps’  $\Delta p = -\underline{E} \cdot \Delta \underline{x}$  over the boundaries. Only the *periodicity directions*  $u, v, w$  are relevant for the boundary conditions. In general the periodicity directions may differ from the Cartesian coordinate directions  $x, y, z$  in which we want to express the homogenized mobility components  $K_{xx}, K_{xy}, K_{xz}, K_{yx}, K_{yy}, K_{yz}, K_{zx}, K_{zy}, K_{zz}$ .

## A.4. SECOND APPLICATION OF BASIC REQUIREMENT

Multiplying the left and right sides of Equation (A.5) by a pressure  $p_1(\underline{x})$ , applying some vector differentiation rules, and using Gauss’s divergence theorem yields

$$\begin{aligned} & \iiint_D \nabla p_1(\underline{x}) \cdot \underline{K} \cdot \nabla P(\underline{x}) \, dV - \iiint_D \nabla p_1(\underline{x}) \cdot \underline{k}(\underline{x}) \cdot \nabla p(\underline{x}) \, dV \\ &= \oiint p_1(\underline{x}) \underline{n} \cdot \underline{K} \cdot \nabla P(\underline{x}) \, dS - \oiint p_1(\underline{x}) \underline{n} \cdot \underline{k}(\underline{x}) \cdot \nabla p(\underline{x}) \, dS, \end{aligned} \quad (\text{A.7})$$

where the circle in the surface integrals means integration over the closed boundary of the periodicity domain. Let us consider the surface integrals in more detail

$$\begin{aligned} I &= - \oiint p_1(\underline{x}) (\underline{k}(\underline{x}) \cdot \nabla p(\underline{x}) - \underline{K} \cdot \nabla P(\underline{x})) \cdot \underline{n} \, dS \\ &= \oiint p_1(\underline{x}) (\underline{q}(\underline{x}) - \underline{Q}) \cdot \underline{n} \, dS. \end{aligned} \quad (\text{A.8})$$

Similar to Equation (A.1), the pressure  $p_1(\underline{x})$  is written as  $p_1(\underline{x}) = c_1 - \underline{E}_1 \cdot \underline{x} + \chi_1(\underline{x})$ . Hence,

$$I = \oiint (c_1 + \chi_1(\underline{x}) - \underline{E}_1 \cdot \underline{x}) (\underline{q}(\underline{x}) - \underline{Q}) \cdot \underline{n} \, dS = I_1 + I_2 + I_3. \quad (\text{A.9})$$

Using Equation (A.5) we find

$$I_1 = c_1 \iint (\underline{q}(\underline{x}) - \underline{Q}) \cdot \underline{n} \, dS = c_1 \iiint_D \nabla \cdot (\underline{q}(\underline{x}) - \underline{Q}) \, dV = 0. \quad (\text{A.10})$$

Using the periodicity of  $\chi_1$  and  $\underline{n} \cdot \underline{q}$  we find

$$I_2 = \iint \chi_1(\underline{x}) (\underline{q}(\underline{x}) - \underline{Q}) \cdot \underline{n} \, dS = 0 \quad (\text{A.11})$$

The evaluation of  $I_3$  is more complex, but also more rewarding.

$$\begin{aligned} I_3 &= \iint \underline{E}_1 \cdot \underline{x} (\underline{q}(\underline{x}) - \underline{Q}) \cdot \underline{n} \, dS \\ &= \underline{E}_1 \cdot \left( \underline{Q}V - \iiint_D \underline{q}(\underline{x}) \, dV \right). \end{aligned} \quad (\text{A.12})$$

When we require  $I_3 = 0$  we find the equivalent of Equation (A.4)

$$\underline{Q} = \frac{1}{V} \iiint_D \underline{q}(\underline{x}) \, dV = \langle \underline{q} \rangle, \quad (\text{A.13})$$

which proves that the homogenized flux is equal to the volume average of the fine-scale flux. Hence, the surface integral in Equation (A.7) is equal to zero, yielding

$$\langle \underline{e}_1 \rangle \cdot \underline{K} \cdot \langle \underline{e} \rangle = \frac{1}{V} \iiint_D \underline{e}_1(\underline{x}) \cdot \underline{q}(\underline{x}) \, dV = \langle \underline{e}_1 \cdot \underline{q} \rangle. \quad (\text{A.14})$$

#### A.5. DISSIPATION

If we choose  $\langle \underline{e} \rangle = \langle \underline{e}_1 \rangle$ , the right-hand side of Equation (A.14) represents the volume averaged dissipation  $\Phi_{11} = \langle \phi_{11} \rangle = \langle \underline{e}_1 \cdot \underline{q}_1 \rangle$ . If we choose  $\langle \underline{e}_1 \rangle = \langle \underline{e}_i \rangle \neq \langle \underline{e} \rangle = \langle \underline{e}_j \rangle$ , we may call the right-hand side of Equation (A.14) the averaged dissipation component  $\Phi_{ij} = \langle \phi_{ij} \rangle = \langle \underline{e}_i \cdot \underline{q}_j \rangle$ .

Since the fine-scale mobility tensor is symmetric, it follows that the matrix of fine-scale dissipation components is symmetric too, that is,  $\phi_{ij}(\underline{x}) = \phi_{ji}(\underline{x})$ , from which it follows that the homogenized mobility tensor is symmetric. Moreover, since the fine-scale mobility tensor is positive definite, it follows that the main diagonal components of the homogenized dissipation are positive, that is,  $\Phi_{ii} > 0$  (no summation over  $i$ ) for  $\underline{e}(\underline{x}) \neq 0$ . This holds in any coordinate system, hence also in the principal coordinate system, from which it follows that the homogenized mobility tensor is positive definite.

## Appendix B

### B.1. INTRODUCTION

A symmetric positive definite mobility tensor  $\underline{\underline{K}}$  has an inverse, here called the resistivity tensor  $\underline{\underline{R}} = \underline{\underline{K}}^{-1}$ . The components of these two tensors can be expressed in a principal coordinate system, with coordinates  $x_1^{(p)}, x_2^{(p)}, x_3^{(p)}$ , in which the matrices of  $\underline{\underline{K}}$  and  $\underline{\underline{R}}$  have the diagonal forms

$$\begin{pmatrix} K_1 & 0 & 0 \\ 0 & K_2 & 0 \\ 0 & 0 & K_3 \end{pmatrix}, \text{ respectively } \begin{pmatrix} R_1 & 0 & 0 \\ 0 & R_2 & 0 \\ 0 & 0 & R_3 \end{pmatrix} = \begin{pmatrix} K_1^{-1} & 0 & 0 \\ 0 & K_2^{-1} & 0 \\ 0 & 0 & K_3^{-1} \end{pmatrix} \quad (\text{B.1})$$

with  $K_1 > 0, K_2 > 0, K_3 > 0$ . Let us consider tensor  $\underline{\underline{S}}$ , for which either tensor  $\underline{\underline{K}}$  or tensor  $\underline{\underline{R}}$  may be substituted. The same tensor  $\underline{\underline{S}}$  written in a system with coordinates  $x_1^{(1)}, x_2^{(1)}, x_3^{(p)}$  obtained by rotation of the principal coordinate system over an angle  $-\varphi$  in the  $x_1^{(p)}x_2^{(p)}$  plane (i.e., the rotation is around the  $x_3^{(p)}$  axis), is given by the following matrix of components (Morse and Feshbach, 1953, pp. 61–63)

$$\begin{aligned} & \begin{pmatrix} \cos \varphi & -\sin \varphi & 0 \\ \sin \varphi & \cos \varphi & 0 \\ 0 & 0 & 1 \end{pmatrix} \cdot \begin{pmatrix} S_1 & 0 & 0 \\ 0 & S_2 & 0 \\ 0 & 0 & S_3 \end{pmatrix} \cdot \begin{pmatrix} \cos \varphi & \sin \varphi & 0 \\ -\sin \varphi & \cos \varphi & 0 \\ 0 & 0 & 1 \end{pmatrix} \\ &= \begin{pmatrix} S_1 \cos^2 \varphi + S_2 \sin^2 \varphi & (S_1 - S_2) \cos \varphi \sin \varphi & 0 \\ (S_1 - S_2) \cos \varphi \sin \varphi & S_1 \sin^2 \varphi + S_2 \cos^2 \varphi & 0 \\ 0 & 0 & S_3 \end{pmatrix} \\ &= \begin{pmatrix} S_{11}^{(1)} & S_{12}^{(1)} & 0 \\ S_{12}^{(1)} & S_{22}^{(1)} & 0 \\ 0 & 0 & S_3 \end{pmatrix}. \end{aligned} \quad (\text{B.2})$$

Again, the tensor  $\underline{\underline{S}}$  written in a system with coordinates  $x_1^{(2)}, x_2^{(1)}, x_3^{(2)}$  obtained by rotation of coordinate system  $x_1^{(1)}, x_2^{(1)}, x_3^{(p)}$  one over an angle  $-\vartheta$  in the  $x_3^{(p)}x_1^{(1)}$  plane (i.e., the rotation is around the  $x_2^{(1)}$  axis), is given by the following matrix of

components:

$$\begin{aligned}
 & \begin{pmatrix} \cos \vartheta & 0 & -\sin \vartheta \\ 0 & 1 & 0 \\ \sin \vartheta & 0 & \cos \vartheta \end{pmatrix} \cdot \begin{pmatrix} S_{11}^{(1)} & S_{12}^{(1)} & 0 \\ S_{12}^{(1)} & S_{22}^{(1)} & 0 \\ 0 & 0 & S_3 \end{pmatrix} \cdot \begin{pmatrix} \cos \vartheta & 0 & \sin \vartheta \\ 0 & 1 & 0 \\ -\sin \vartheta & 0 & \cos \vartheta \end{pmatrix} \\
 &= \begin{pmatrix} S_{11}^{(1)} \cos^2 \vartheta + S_3 \sin^2 \vartheta & S_{12}^{(1)} \cos \vartheta & (S_{11}^{(1)} - S_3) \cos \vartheta \sin \vartheta \\ S_{12}^{(1)} \cos \vartheta & S_{22}^{(1)} & S_{12}^{(1)} \sin \vartheta \\ (S_{11}^{(1)} - S_3) \cos \vartheta \sin \vartheta & S_{12}^{(1)} \vartheta & S_{11}^{(1)} \sin^2 \vartheta + S_3 \cos^2 \vartheta \end{pmatrix} \\
 &= \begin{pmatrix} S_{11}^{(2)} & S_{12}^{(2)} & S_{13}^{(2)} \\ S_{12}^{(2)} & S_{22}^{(1)} & S_{23}^{(2)} \\ S_{31}^{(2)} & S_{23}^{(2)} & S_{33}^{(2)} \end{pmatrix}. \tag{B.3}
 \end{aligned}$$

For the calculation of the homogenized mobility tensor  $\underline{K}$ , or its inverse  $\underline{R}$ , any convenient coordinate system may be chosen. For instance, the ‘natural’ directions of the periodic fine-scale mobility distribution may be chosen as coordinate axes. Let us denote the coordinates of the chosen coordinate system by  $x, y, z$ . Since any rotation can be described by at most three subsequent rotations over three different axes, a third rotation is needed to obtain this  $x, y, z$  system. Therefore, we rotate the coordinate system  $x_1^{(2)}, x_2^{(1)}, x_3^{(2)}$  over an angle  $-\psi$  in the  $x_2^{(1)}x_3^{(2)}$  plane (i.e., the rotation is around the  $x_1^{(2)}$  axis). Then the matrix of components is given by

$$\begin{pmatrix} 1 & 0 & 0 \\ 0 & \cos \psi & -\sin \psi \\ 0 & \sin \psi & \cos \psi \end{pmatrix} \cdot \begin{pmatrix} S_{11}^{(2)} & S_{12}^{(2)} & S_{13}^{(2)} \\ S_{12}^{(2)} & S_{22}^{(1)} & S_{23}^{(2)} \\ S_{13}^{(2)} & S_{23}^{(2)} & S_{33}^{(2)} \end{pmatrix} \cdot \begin{pmatrix} 1 & 0 & 0 \\ 0 & \cos \psi & \sin \psi \\ 0 & -\sin \psi & \cos \psi \end{pmatrix} \tag{B.4}$$

from which it follows that the components of the *main diagonal* are given by

$$\begin{pmatrix} S_{xx} \\ S_{yy} \\ S_{zz} \end{pmatrix} = \begin{pmatrix} S_{11}^{(2)} \\ S_{22}^{(1)} \cos^2 \psi - 2S_{23}^{(2)} \cos \psi \sin \psi + S_{33}^{(2)} \sin^2 \psi \\ S_{22}^{(1)} \sin^2 \psi + 2S_{23}^{(2)} \cos \psi \sin \psi + S_{33}^{(2)} \cos^2 \psi \end{pmatrix}. \tag{B.5}$$

Summation of these components yields the trace of the matrix

$$T = S_{xx} + S_{yy} + S_{zz} = S_1 + S_2 + S_3 > 0, \tag{B.6}$$

which shows that the trace of a matrix is invariant under coordinate transforms. Hence, the trace is a tensor property.

In addition, since  $S_1 > 0, S_2 > 0, S_3 > 0$ , we find from Equation (B.5)

$$S_{xx} = S_1 \cos^2 \vartheta \cos^2 \vartheta + S_2 \sin^2 \vartheta \cos^2 \vartheta + S_3 \sin^2 \vartheta > 0 \tag{B.7}$$

and in a similar way (section B.2.) it can be proved that also  $S_{yy} > 0$  and  $S_{zz} > 0$ .

### B.2. ERROR ESTIMATES BASED ON THE TRACES

Let us now consider numerical approximations  $\hat{S}_1, \hat{S}_2, \hat{S}_3$  of the exact principal mobilities or resistivities  $S_1, S_2, S_3$ . Then, according to Equation (A.6) the following expression holds

$$\hat{T} = \hat{S}_{xx} + \hat{S}_{yy} + \hat{S}_{zz} = \hat{S}_1 + \hat{S}_2 + \hat{S}_3. \quad (\text{B.8})$$

Subtraction of Equation (B.6) and (B.8) yields

$$\Delta T = \Delta S_{xx} + \Delta S_{yy} + \Delta S_{zz} = \Delta S_1 + \Delta S_2 + \Delta S_3, \quad (\text{B.9})$$

where  $\Delta T = \hat{T} - T$ ,  $\Delta S_{xx} = \hat{S}_{xx} - S_{xx}$ , etc. We have mentioned in Section 5 that CN-FEM approximations yield principal mobilities that are too large, while MH-FEM approximations yield principal mobilities that are too small. Then it follows from Equation (B.9) that CN-FEM approximations yield a sum of the diagonal mobilities that is too large, while MH-FEM approximations yield a sum of the diagonal mobilities that is too small. Similarly, it follows from Equation (B.9) that CN-FEM approximations yield a sum of the diagonal resistivities that is too small, while MH-FEM approximations yield a sum of the diagonal resistivities that is too large. Since this holds true in any coordinate system, not only in the principal coordinate system, both the sum of the diagonal mobility components and the sum of the diagonal resistivity components, can be used as error estimates.

### B.3. INDIVIDUAL DIAGONAL MOBILITIES AS ‘SOFT’ ERROR ESTIMATES

For reasons that will be made clear later, we define the first, second and third rotation angles as  $\varphi_1 = \varphi$ ,  $\vartheta_1 = \vartheta$ , and  $\psi_1 = \psi$ , respectively. As has been explained above, these rotations are chosen in such a way that the first rotation is around the 3-axis, the second rotation is around the 2-axis, and the last rotation is around the 1-axis. Under the assumption that  $\hat{\varphi} = \varphi$ ,  $\hat{\vartheta} = \vartheta = \vartheta$ ,  $\hat{\psi} = \psi$  (see below), we find from Equation (B.7)

$$\Delta K_{xx} = \Delta K_1 \cos^2 \varphi_1 \cos^2 \vartheta_1 + \Delta K_2 \sin^2 \varphi_1 \cos^2 \vartheta_1 + \Delta K_3 \sin^2 \vartheta_1. \quad (\text{B.10})$$

Now the first, second and third rotation angles are chosen as  $\varphi_2, \vartheta_2, \psi_2$ , respectively, in such a way that the first rotation is around the 1-axis, the second rotation is around the 3-axis, and the last rotation is around the 2-axis. Then we find in a similar way

$$\Delta K_{yy} = \Delta K_2 \cos^2 \varphi_2 \cos^2 \vartheta_2 + \Delta K_3 \sin^2 \varphi_2 \cos^2 \vartheta_2 + \Delta K_1 \sin^2 \vartheta_2. \quad (\text{B.11})$$

Finally, the first, second and third rotation angles are chosen as respectively  $\varphi_3, \vartheta_3, \psi_3$ , in such a way that the first rotation is around the 2-axis, the second rotation is around the 1-axis, and the last rotation is around the 3-axis. Then we find

$$\Delta K_{zz} = \Delta K_3 \cos^2 \varphi_3 \cos^2 \vartheta_3 + \Delta K_1 \sin^2 \varphi_3 \cos^2 \vartheta_3 + \Delta K_2 \sin^2 \vartheta_3. \quad (\text{B.12})$$

The results of the numerical approximations give often the impression that the directions of the preferential flow paths, which are characterized by  $\varphi$ ,  $\vartheta$ ,  $\psi$ , are calculated sufficiently accurate. Therefore, we consider conditions where the approximate principal directions are sufficiently accurate (i.e.,  $\hat{\varphi} - \varphi = 0$ ,  $\hat{\vartheta} - \vartheta = 0$ ,  $\hat{\psi} - \psi = 0$ ). As has been explained before, the approximate principal mobilities are too large for CN-FEM and too small for MH-FEM. Then it follows from Equations (B.10), (B.11) and (B.12) that the diagonal mobilities are too high (CN-FEM) or too low (MH-FEM) in any coordinate system; not only in the principal coordinate system. This means that each of the three diagonal components may be used as an additional, 'soft' error estimate.

## References

- Aavatsmark, I., Barkve, T., Bøe, Ø. and Mannseth, T.: 1996, Discretization on non-orthogonal, quadrilateral grids for inhomogeneous, anisotropic media *J. Comput. Phys.* **127**, 2–14.
- Auriault, J.-L.: 1983, Effective macroscopic description for heat conduction in periodic composites *Int. J. Heat and Mass Transfer* **26**(6), 861–869.
- Barenblatt, G. I., Entov, V. M. and Ryzhik, V. M.: 1990, *Theory of Fluid Flows Through Natural Rocks*, Kluwer Academic Publishers, Dordrecht.
- Bensoussan, A., Lions, J.-L. and Papanicolau, G.: 1978, *Asymptotic Analysis for Periodic Structures*, North Holland Publishing Company, Amsterdam.
- Bentsen, R. G.: 1994, An investigation into whether the nondiagonal mobility coefficients which arise in coupled, two phase flow are equal, *Transport in Porous Media* **14**, 23–32.
- Bøe, Ø.: 1994, Analysis of an upscaling method based on conservation of dissipation, *Transport in Porous Media* **17**, 77–86.
- Case, C. M.: 1994, *Physical Principles of Flow in Unsaturated Porous Media*, Oxford University Press, New York.
- Durllofsky, L. J.: 1992, Modeling fluid flow through complex reservoir beds, *SPE Formation Evaluation* Dec., 315–322.
- Duvaut, G. and Lions, J.-L.: 1976, *Inequalities in Mechanics and Physics*, Springer-Verlag, Berlin.
- Hornung, U.: 1997, *Homogenization and Porous Media*, Springer-Verlag, Berlin.
- Kaasschieter, E. F. and Huijben, A. J. M.: 1992, Mixed-hybrid finite elements and streamline computations for potential flow problems, *Numerical Methods for Partial Differential Equations* **8**, 221–246.
- King, M. J., King, P. R., McGill, C. A. and Williams, J. K.: 1995, Effective properties for flow calculations, *Transport in Porous Media* **20**, 169–196.
- Knapek, S.: 1998, Upscaling techniques based on subspace corrections and coarse-grid approximations, *In Situ* **20**(1), 35–58.
- Morse, Ph. M. and Feshbach, H.: 1953, *Methods of Theoretical Physics*, McGraw-Hill, New York.
- Panfilov, M.: 1992, Structural averaging of porous flow processes in heterogeneous media, *Fluid Dynamics* **3**, 112–120.
- Penman, J.: 1988, Dual and complementary variational techniques for the calculation of electromagnetic fields, *Advances in Electronics and Electron Physics* **70**, 315–364.
- Quintard, M. and Whitaker, S.: 1988, Two-phase flow in heterogeneous porous media: the method of large-scale averaging, *Transport in Porous Media* **3**, 357–413.
- Ribeiro, R. F. and Romeu, R. K.: 1997, Computing the effective permeability by finite differences, finite elements, and mixed-hybrid finite elements, *SPE* 39068.
- Sanchez-Palencia, E.: 1980, *Non-Homogeneous Media and Vibration Theory*, in: Lecture Notes in Physics 127, Springer-Verlag, Berlin.

- Trykozko, A. and Zijl, W.: 1999, *From Fine-Scale to Coarse-Scale Permeability by Numerical Homogenization and Volume Averaging (Part I & II)*, Netherlands Institute of Applied Geoscience, report no. 99-5-B, Utrecht.
- Warren, J. E. and Price, H. S.: 1961, Flow in heterogeneous porous media, *SPE J* Sept., 153–169.
- Zijl, W. and Trykozko, A.: 1999, *From Fine-Scale to Coarse-Scale Permeability by Homogenization and Volume Averaging*, Netherlands Institute of Applied Geoscience, report no. 99-4-B, Utrecht.
- Zijl, W. and Nawalany, M.: 1993, *Natural Groundwater Flow*, Lewis/CRC Publishing Comp., Inc., Boca Raton.